

Intrinsic Rotation of a Magnetic Island with Finite Width

Ken UZAWA, Akihiro ISHIZAWA and Noriyoshi NAKAJIMA

National Institute for Fusion Science, 322-6 Oroshi-cho Toki-city, Gifu 509-5292, Japan

(Received 19 January 2009 / Accepted 14 July 2009)

The rotation direction of a magnetic island in the saturation regime and the underlying physical mechanism are numerically investigated based on a four-field model that includes the effects of both ion and electron diamagnetic drifts as well as parallel ion motion. It is found that diamagnetic effects vanish inside the island, and that the rotation direction is determined by nonlinearly generated zonal flow. The direction of zonal flow is sensitive to the viscosity and the finite Larmor radius (FLR) effect. The radial mode structure of zonal flow is found to be deformed by that of other modes as the viscosity increases. We have also shown that the FLR effect enhances island rotation toward the ion diamagnetic drift direction through energy transfer to the zonal flow by a nonlinear ion diamagnetic stress tensor.

© 2010 The Japan Society of Plasma Science and Nuclear Fusion Research

Keywords: island rotation, neoclassical tearing mode, two fluid model, zonal flow

DOI: 10.1585/pfr.5.S1016

1. Introduction

Tearing modes are resistive magnetohydrodynamic (MHD) instabilities that break the topology of the ideal magnetic field and lead to the formation of helically perturbed structures called magnetic islands by tearing or reconnecting magnetic field lines around the resonant surfaces in magnetic confinement devices. Linear theory shows that the classical tearing mode is stable when the stability parameter

$$\Delta' = \frac{1}{\tilde{\psi}} \left[\left. \frac{d\tilde{\psi}}{dx} \right|_{x=+0} - \left. \frac{d\tilde{\psi}}{dx} \right|_{x=-0} \right]$$

is negative, which is given by a logarithmic jump of the perturbed magnetic flux around the rational surface [1]. However, in recent low-collisional plasmas, a new type of tearing modes, sustained by helically perturbed bootstrap current, can occur even when classically stable (i.e., the stability parameter is negative). The metastable (linearly stable but nonlinearly unstable) tearing modes are called neoclassical tearing modes (NTMs). NTMs are found to limit the achievable beta in high-performance discharges and deteriorate plasma confinement, leading to plasma disruption. Therefore, much attention has been focused on NTMs both theoretically and experimentally [2–4].

To understand NTM dynamics theoretically, the modified Rutherford equation is often used as the model equation describing temporal evolution of magnetic island width,

$$\frac{\tau_s}{r_s} \frac{dw}{dt} = r_s \Delta' + \beta_p \left(\frac{\Delta_b w}{w^2 + w_0^2} - \frac{\Delta_p}{w^3} \right),$$

where $\tau_s = \mu_0 r_s^2 / 1.22\eta$ is the resistive diffusion time at the magnetic surface of radius r_s , η is the neoclassical re-

author's e-mail: uzawa.ken@nifs.ac.jp

sistivity, Δ' is the classical tearing stability parameter discussed above, β_p is the poloidal beta at r_s , and w_0 is the characteristic island width. The two parameters, Δ_b and Δ_p represent the effects of the bootstrap and polarization currents, respectively. When the sign of Δ_p is positive, the polarization term enhances NTM growth. As a typical representation, Δ_p is written as

$$\Delta_p = \frac{L_s^2}{k v_A^2} \Omega (\Omega - \omega_{*i}),$$

where Ω is the island rotation frequency, ω_{*i} is the ion diamagnetic drift frequency, L_s is the magnetic shear length, k is the wave number of the mode, and $v_A = \sqrt{B_0^2 / 4\pi n m_i}$ is the Alfvén velocity [5, 6]. When the island propagates toward the electron (ion) diamagnetic drift, the sign of the polarization term is positive (negative). Therefore, determining the propagation direction of the island is important for evaluating NTM growth. However, the effects of parallel ion motion and ion diamagnetic drift motion are neglected in these models. Actually, the ion temperature in realistic plasmas is of the order of the electron temperature, so the cold assumption for ions seems to be incorrect. To evaluate the propagation direction of the island more correctly, we have to include these effects in the model equations. For this purpose, we investigate the direction of island rotation in the saturation regime here. The physical mechanism of directional change is also discussed. We found that in some situations, the island can rotate toward the ion diamagnetic drift direction in the nonlinear regime. This behavior originates from the disappearance of diamagnetic drifts due to pressure flattening inside the island and the generation of zonal flow in the nonlinear regime. We have also shown that the viscosity and finite Larmor radius (FLR) effect are important in determining the island

direction.

The remainder of this work is organized as follows. In Sec. 2 we present the model equations used here. Numerical simulation results are presented in Sec. 3. In Sec. 4, island rotation in the nonlinear regime and the differences from the linear result are discussed. The mechanism of changes in the island rotation direction is also investigated. We have shown that finally, the island rotates in the nonlinearly generated zonal flow. Ion parallel motion is found to contribute to pressure flattening. Finally, the conclusion is given in Sec. 5.

2. Model Equations

Since there is no degree of freedom determining island rotation in conventional MHD models, we have investigated the rotation of an island based on a reduced two-fluid model that includes the effects of both ion and electron diamagnetic drifts. The model equations used here represent a two-dimensional slab version of the four-field model [7], which consists of a set of four equations that describe temporal evolution of the magnetic flux ψ , the electrostatic potential ϕ , the perturbed electron pressure p , and the parallel ion velocity v_{\parallel} , i.e.,

$$\begin{aligned} \frac{\partial U}{\partial t} &= -[\varphi, U] - \nabla_{\parallel} J + \nu \nabla_{\perp}^2 U \\ &\quad - \frac{\delta \tau}{2} ([p, U] + [\varphi, \nabla_{\perp}^2 p] + \nabla_{\perp}^2 [p, \varphi]), \\ \frac{\partial \psi}{\partial t} &= -\nabla_{\parallel} \varphi + \eta J + \delta \nabla_{\parallel} p, \\ \frac{\partial p}{\partial t} &= -[\varphi, p] - 2\beta \delta \nabla_{\parallel} J - \beta \nabla_{\parallel} v \\ &\quad + \frac{1}{2} \beta \eta (1 + \tau) \nabla_{\perp}^2 p, \\ \frac{\partial v}{\partial t} &= -[\varphi, v] - \frac{1}{2} (1 + \tau) \nabla_{\parallel} p + D_v \nabla_{\perp}^2 v, \end{aligned}$$

with vorticity $U = \nabla_{\perp}^2 \phi$, and z -directed current density $J = \nabla_{\perp}^2 \psi$. The usual Cartesian coordinates (x, y, z) are adopted. The validity of two-dimensional calculation is justified in low-beta plasmas, where the magnetic field is represented by $\mathbf{B} = B_0 \hat{z} + \nabla \psi \times \hat{z}$, where B_0 is the ambient magnetic field along the z -axis. The normalization used here is $(x, y, t, \psi, \phi, n, v_{\parallel i}) = (x/a, y/a, v_A t/a, \psi/\varepsilon B_0 a, c\phi/v_A B_0 a, n/n_0, \delta v_{\parallel i}/v_A)$. Here, a and R are the minor and major radii, respectively. c is light speed, $\varepsilon = a/R$ is the inverse aspect ratio, ν is the viscosity, η is the resistivity, and both the equilibrium ion and electron density n_0 are constant due to charge neutrality. We suppose that the ion and electron temperatures are constant by introducing their ratio $\tau = T_i/T_e$. The normalized parameters δ and β are introduced as two fluid parameters. The former is related to the ion skin depth $\delta = (2\omega_{ci}\tau_A)^{-1}$, where $\omega_{ci} = \sqrt{eB_0/cm_i}$ is the ion cyclotron frequency, and $\tau_A = a/v_A$ is the poloidal Alfvén transit time. The latter is $\beta = \beta_e [1 + \beta_e(1 + \tau)/2]^{-1}$, where $\beta_e = 8\pi n_0 T_e/B_0^2$ is the electron plasma beta. One can find

that the ion Larmor radius is related to the cross product of these two parameters, i.e., $(\rho_i/a)^2 = 2\tau\delta^2\beta_e$. The operator $[\cdot, \cdot]$ denotes the Poisson bracket, $[A, B] = \nabla_{\perp} A \times \nabla_{\perp} B \cdot \hat{z}$.

3. Linear Calculation

3.1 Numerical settings

In this research, we adopt two-dimensional slab geometry as an approximate model for the tokamak geometry. Although, we cannot consider an internal kink mode in the slab model, here we focus on the tearing mode that occurs near the magnetic neutral sheet far from plasma boundaries. Generally, the slab model can capture mainly the most dominant dynamics.

The model equations are solved numerically by using pseudo spectral code. We impose the zero boundary condition for radial direction x , so all components are automatically set to zero at the radial boundary. A finite-differential method is applied in the radial direction, and a periodic boundary condition is imposed for the poloidal direction y . The domain of the numerical simulations is $x = [0, 1]$ and $y = [0, 1]$. The number of grids in a simulation box is 400×20 . Temporal evolution is calculated by using a predictor-corrector method with time step $\Delta t = 10^{-3}$. The pressure and magnetic flux equilibrium profiles are $p_{\text{eq}}(x) = 0.25(1 - \tanh(x - 0.5))/L_p$, and $\psi_{\text{eq}}(x) = L_s \ln[\cosh(x - 0.5)/L_s]$. We have no equilibrium parts for either electrostatic potential ϕ or ion parallel velocity v , i.e., $\phi = \tilde{\phi}$, $v = \tilde{v}$. All calculations described in this article are performed with $\nu = 10^{-6} \sim 10^{-4}$, $\eta = 10^{-4}$, and $D_v = 10^{-4}$. These numerical values may be large compared to the realistic transport coefficients in tokamak plasmas, and these higher values correspond to hyperviscosity in the numerical calculations. This situation is suitable if these coefficients include the effects of interaction between the island and microscale turbulence. A temperature ratio of unity $\tau = 1$ is chosen, and the shear and density scale lengths are set to $L_s = 0.1$ and $L_p = 0.15$, respectively. The stability parameter Δ' is positive only for the $m = 1$ mode, and the other modes are all linearly stable. From now on, we discuss the rotation frequency of the $m = 1$ mode.

3.2 Linear results

First, we examine island rotation by performing linear calculation. All perturbed quantities $\tilde{A}(x, y, t)$ are assumed to vary as

$$\tilde{A}(x, y, t) = \sum_m A_m(x) \exp[i(2\pi m y - \omega_m t)],$$

where m is the poloidal mode number, $\omega_m = i\gamma_m + \Omega_m$ is the complex frequency, γ_m is the growth rate, and Ω_m is the rotation (angular) frequency. Note that the island rotates toward the electron diamagnetic drift frequency when Ω_m is positive. The linearized equations are

$$\frac{\partial U_m}{\partial t} = \frac{\partial \psi_{\text{eq}}}{\partial x} \frac{\partial J_m}{\partial y} - \frac{\partial \psi_m}{\partial y} \frac{\partial J_{\text{eq}}}{\partial x} + \nu \nabla_{\perp}^2 U_m$$

$$\begin{aligned}
 & + \delta\tau \left(-\frac{\partial p_{\text{eq}}}{\partial x} \frac{\partial U_m}{\partial y} - \frac{\partial^2 p_{\text{eq}}}{\partial x^2} \frac{\partial^2 \varphi_m}{\partial x \partial y} \right), \\
 \frac{\partial \psi_m}{\partial t} & = \frac{\partial \psi_{\text{eq}}}{\partial x} \frac{\partial \varphi_m}{\partial y} + \eta \nabla_{\perp}^2 \psi_m \\
 & + \delta \left(-\frac{\partial \psi_{\text{eq}}}{\partial x} \frac{\partial p_m}{\partial y} + \frac{\partial p_{\text{eq}}}{\partial x} \frac{\partial \psi_m}{\partial y} \right), \\
 \frac{\partial p_m}{\partial t} & = \frac{\partial p_{\text{eq}}}{\partial x} \frac{\partial \varphi_m}{\partial y} + 2\beta\delta \left(\frac{\partial \psi_{\text{eq}}}{\partial x} \frac{\partial J_m}{\partial y} - \frac{\partial J_{\text{eq}}}{\partial x} \frac{\partial \psi_m}{\partial y} \right) \\
 & + \beta \frac{\partial \psi_{\text{eq}}}{\partial x} \frac{\partial v_m}{\partial y} + \frac{\beta\eta}{2} (1 + \tau) \nabla_{\perp}^2 (p_{\text{eq}} + p_m), \\
 \frac{\partial v_m}{\partial t} & = \frac{1 + \tau}{2} \left(\frac{\partial \psi_{\text{eq}}}{\partial x} \frac{\partial p_m}{\partial y} - \frac{\partial p_{\text{eq}}}{\partial x} \frac{\partial \psi_m}{\partial y} \right) + D_v \nabla_{\perp}^2 v_m.
 \end{aligned}$$

We can control the strength of the magnetic field B_0 in plasmas by changing β . In Fig. 1, the rotation frequency of the $m = 1$ mode Ω ($\equiv \Omega_1$) is illustrated as a function of β for various δ . When δ is large, the rotation frequency becomes small, indicating that the FLR effect enhances island rotation in the direction of ion diamagnetic drift. Compared to δ , β dependence is found to be small. As shown in these results, the island rotates toward electron diamagnetic drift in the linear regime.

4. Nonlinear Calculation

In the previous section, we found that in the linear regime the island rotates toward the electron diamagnetic drift direction. However, in the regime where the island width is quite large as compared to the linear tearing layer width, the linear theory may be invalid. The NTM is intrinsically a nonlinear instability, therefore it is important to know the direction of island rotation where the nonlinearity is important. In this section, we discuss the island propagation direction in the nonlinear regime.

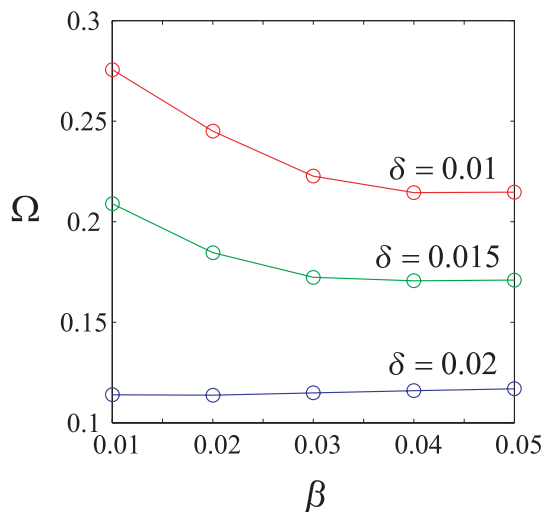


Fig. 1 Rotation frequency as a function of β for various δ .

4.1 Propagation direction in the nonlinear regime

Figure 2 shows the temporal evolution of the rotation frequency (blue line) and width (red line) of the island. The rotation frequency and width are normalized by the linear electron diamagnetic frequency and minor radius, respectively. In accordance with the linear results, the island initially propagates toward the electron diamagnetic drift. Since island rotation in the electron diamagnetic direction is weakened by the linear ion diamagnetic drift effect, the rotation frequency is small compared to the linear electron diamagnetic drift frequency. As the island width exceeds the linear tearing layer width and nonlinearity becomes effective, rotation toward the electron diamagnetic drift direction gradually weakens. We can observe that at around $t = 260$, the rotation direction changes. Finally, when island growth reaches the saturate state, the island rotates toward the ion diamagnetic drift direction.

4.2 Propagation with the zonal flow

In the preceding subsection we found that the island can rotate toward the ion diamagnetic drift direction in the nonlinear regime. Here, we consider the mechanism of the rotation change in detail.

Figure 3 shows the temporal evolution of island poloidal velocity and drift velocities. The red line represents the poloidal velocity of the island, the green one is the electron diamagnetic velocity, the blue one is the zonal flow velocity, and the orange one is the sum of the electron diamagnetic and zonal flow velocities. Note that each velocity is averaged over the flux surface. Initially, the island propagates toward the electron diamagnetic direction. We found that as the island width increases, the pressure is flattened inside the island. After about $t = 200$, the flattening begins to have an effect and the electron diamagnetic drift weakens. Finally, the pressure is totally flattened inside the island. On the other hand, the zonal flow is nonlinearly

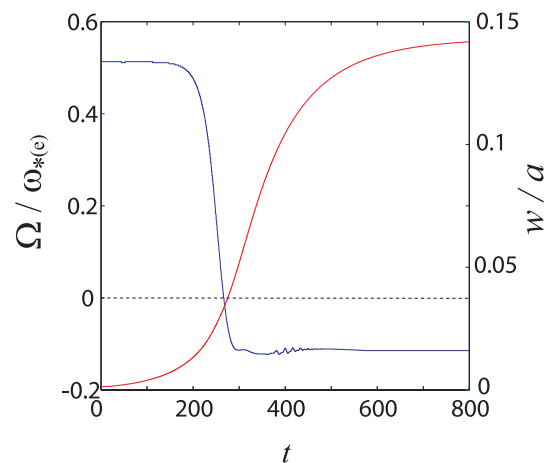


Fig. 2 Temporal evolution of the rotation frequency (blue line) and width (red line) of the island.

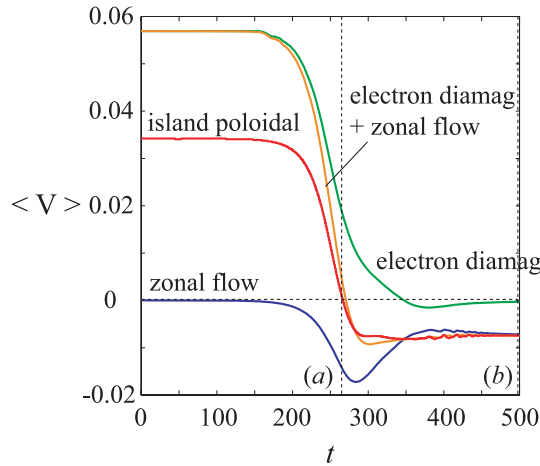


Fig. 3 Temporal evolution of island poloidal velocity (red line), electron diamagnetic velocity (green line), zonal flow velocity (blue line), and the sum of the electron diamagnetic and zonal flow velocities (orange line).

generated. We find that the poloidal velocity is the sum of the electron diamagnetic drift and zonal flow velocities. Eventually, as mentioned earlier, the pressure gradient is flattened, so the island propagates with the zonal flow.

Snapshots of current density and pressure at two different times, (a) $t = 267$ and (b) $t = 500$ are shown in Fig. 4. The separatrix (dotted line) is also plotted as a reference. Here, $\eta = 10^{-4}$, $\nu = 5 \times 10^{-6}$, $\delta = 0.02$, $\beta = 0.05$, and $\tau = 1.0$. The horizontal and vertical axes (x , y) represent the radial and poloidal directions, respectively. The magnetic neutral sheet lies at $x = 0.5$. A uniform magnetic field B_0 lies along the z -axis. Since the pressure gradient is along the radial direction, the electron (ion) diamagnetic drift moves upward (downward). In case (a), where the island rotation is locked, the pressure is partially flattened in the island. In case (b), the current density is found to show complex structure due to excitation of higher modes. We can observe in the saturation regime that the pressure is totally flattened inside the island, whereas a residual pressure profile is observed in traditional models, which do not include the effect of parallel ion motion. We found that parallel ion motion is an important factor in determining the island rotation direction precisely, which is consistent with Ref. [8].

Figure 5 shows the zonal flow velocity in the saturation regime as a function of the viscosity in the saturation regime. The island propagates toward the electron diamagnetic drift in the high-collisional regime where the magnetic Prandtl number $P_r = \nu/\eta$ is approximately unity. The zonal flow velocity monotonically increases with respect to the viscosity. At around $\nu = 2.0 \times 10^{-5}$, the propagation direction changes. The rotation direction is found to depend strongly on the viscosity.

4.3 Energy transfer to zonal flow

In this subsection, we investigate the underlying mechanism of the viscosity dependence of zonal flow ve-

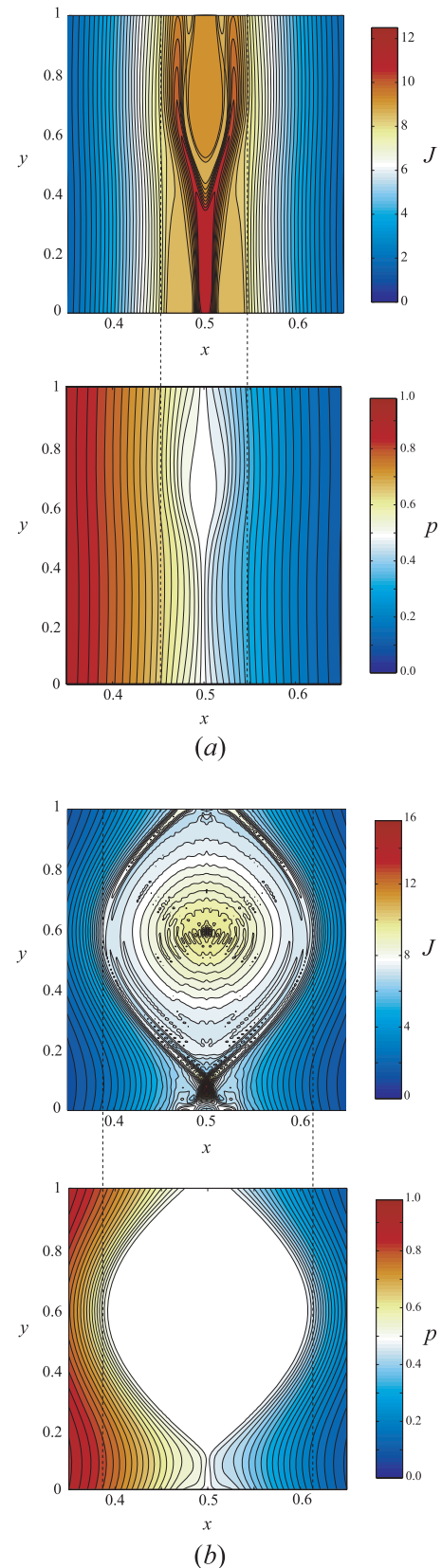


Fig. 4 Contour plots of current density and pressure at two different times, (a) $t = 267$ and (b) $t = 500$.

locity in the saturation regime. Figure 6 shows the temporal evolution of the kinetic energy of each poloidal mode for two viscosity cases, (a) $\nu = 5 \times 10^{-6}$ and (b) $\nu =$

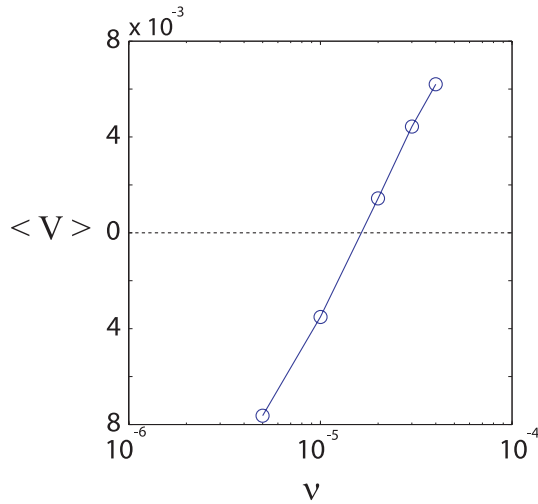


Fig. 5 Zonal flow velocity in the saturation regime as a function of viscosity.

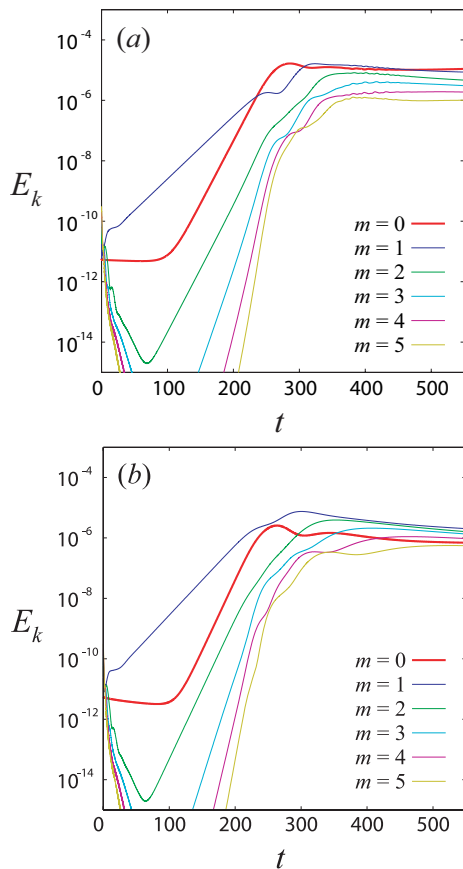


Fig. 6 Temporal evolution of the kinetic energy of each poloidal mode for two different viscosity cases, (a) $\nu = 5 \times 10^{-6}$ and (b) $\nu = 3 \times 10^{-5}$.

3×10^{-5} . In both cases, only the $m = 1$ mode grows in the linear regime. At around $t = 80$, island growth enters the nonlinear phase, and the $m = 0$ mode, i.e., zonal flow, is excited through nonlinear mode coupling. The growth rate of zonal flow is twice that of the $m = 1$ mode, indi-

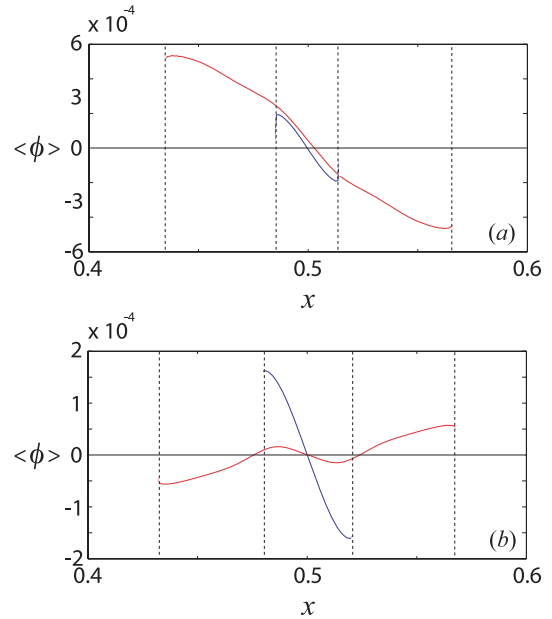


Fig. 7 Radial structures of zonal flow potential inside the island for two viscosity cases, (a) $\nu = 5 \times 10^{-6}$ and (b) $\nu = 3 \times 10^{-5}$ at different times $t = 250$ (blue line) and $t = 550$ (red line).

cating that zonal flow is generated mainly from the $m = 1$ mode. As seen in Fig. 6 (a), the zonal flow finally becomes the most dominant mode in the saturation regime. In contrast, we can observe that in case (b) the zonal flow energy decreases due to viscous damping and the zonal flow energy is the same or smaller than the energy of other modes. In this situation, the mode structure of zonal flow can be affected by that of other modes.

Figure 7 shows the radial structures of zonal flow potential inside the island for two viscosity cases, (a) $\nu = 5 \times 10^{-6}$ and (b) $\nu = 3 \times 10^{-5}$. Two different temporal snapshots, $t = 250$ (blue line) and $t = 550$ (red line), are plotted for each case. The dotted lines indicate the separatrix at a given time. In case (a), the radial mode structure is found to maintain a monotonically decreasing function through the temporal evolution. On the other hand, in case (b), the mode structure reverses its functional form in the saturation regime. This is attributed to deformation of the mode structure of zonal flow by other modes, as expected from Fig. 6 (b).

4.4 The FLR effect on the rotation direction

Here, we investigate the effect of δ on the rotation frequency in the nonlinear regime. Figure 8 shows the rotation frequency as a function of island width for various δ . The viscosity and β are $\nu = 3 \times 10^{-5}$ and $\beta = 0.05$, respectively. The rotation frequency decreases as δ increases through the temporal evolution, suggesting that the FLR effect enhances island rotation toward the ion diamagnetic drift direction. Figure 9 shows the temporal evolution of energy transfer to the zonal flow by nonlinear

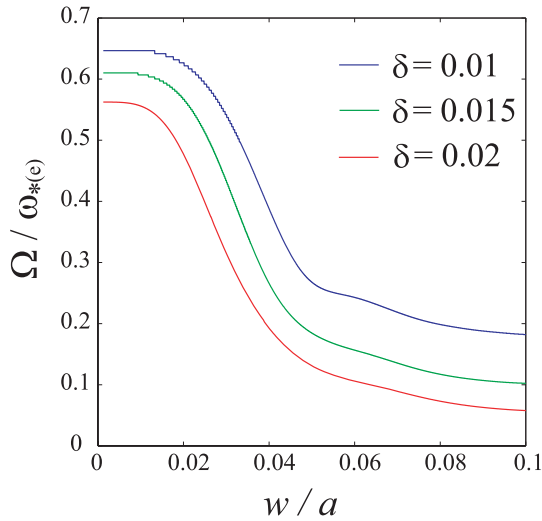


Fig. 8 Rotation frequency as a function of island width for various δ .

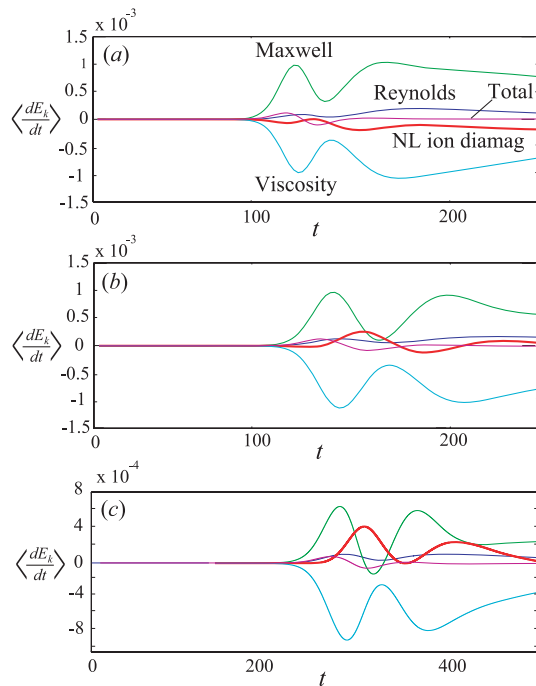


Fig. 9 Temporal evolution of energy transfer to zonal flow by the Reynolds stress (blue line), Maxwell stress (green line), nonlinear ion diamagnetic stress (red line), and viscous stress (cyan line) for (a) $\delta = 0.01$, (b) $\delta = 0.015$, and (c) $\delta = 0.02$.

stresses for three different FLR parameters: (a) $\delta = 0.01$, (b) $\delta = 0.015$, and (c) $\delta = 0.02$. We can observe that as δ increases, the energy transfer to the zonal flow from the nonlinear ion diamagnetic stress increases. We found that zonal flow generation strengthens due to increase of the nonlinear ion diamagnetic stress.

5. Conclusion

In conclusion, we have shown that the pressure is totally flattened inside an island, and the island is carried by nonlinearly generated zonal flow in the saturation regime. This suggests that the rotation direction depends on ion parallel motion, which is not taken into account correctly in conventional models. We found that the rotation direction in the saturation regime is sensitive to the viscosity and the FLR effect. As the viscosity becomes large, island rotation toward the ion diamagnetic drift direction weakens. This is found to originate from deformation of the radial mode structure of the zonal flow by other modes. We have also shown that the FLR effect enhances zonal flow generation, leading to island rotation toward the ion diamagnetic drift direction.

More analyses including neoclassical effects, e.g., the effect of bootstrap current, are necessary. They will be discussed in future work.

Acknowledgments

One of the authors (K. U.) thanks Dr. M. Sato and Dr. S. Nishimura in NIFS for valuable discussions.

- [1] H. P. Furth, J. Killeen and M. N. Rosenbluth, *Phys. Fluids* **6**, 459 (1963).
- [2] R. J. La Haye, *Phys. Plasmas* **13**, 055501 (2006).
- [3] A. Isayama, Y. Kamada, T. Ozeki and N. Isei, *Plasma. Phys. Control. Fusion* **41**, 35 (1999).
- [4] R. Fitzpatrick, *Phys. Plasmas* **2**, 825 (1995).
- [5] J. W. Connor, F. L. Waelbroeck and H. R. Wilson, *Phys. Plasmas* **8**, 2835 (2001).
- [6] R. Fitzpatrick and F. L. Waelbroeck, *Phys. Plasmas* **12**, 022307 (2005).
- [7] R. D. Hazeltine, M. Kotschenreuther and P. J. Morrison, *Phys. Fluids* **28**, 2466 (1985).
- [8] M. Ottaviani, F. Porcelli and D. Grasso, *Phys. Rev. Lett.* **93**, 075001-1 (2004).